

Revisiting Greenland ice sheet mass loss observed by GRACE

Ernst J. O. Schrama¹ and Bert Wouters²

Received 4 August 2009; revised 10 November 2010; accepted 23 November 2010; published 12 February 2011.

[1] In this paper we discuss a new method for determining mass time series for 16 hydrological basins representing the Greenland system (GS) whereby we rely on Gravity Recovery and Climate Experiment (GRACE) mission data. In the same analysis we also considered observed mass changes over Ellesmere Island, Baffin Island, Iceland, and Svalbard (EBIS). The summed contribution of the complete system yields a mass loss rate and acceleration of -252 ± 28 Gt/yr and -22 ± 4 Gt/yr² between March 2003 and February 2010 where the error margins follow from two glacial isostatic adjustment (GIA) models and three processing centers providing GRACE monthly potential coefficient sets. We describe the relation between mass losses in the GS and the EBIS region and found that the uncertainties in all areas are correlated. The summed contribution of Ellesmere Island, Baffin Island, Iceland, and Svalbard yields a mass loss rate of -51 ± 17 Gt/yr and an acceleration of -13 ± 3 Gt/yr² between March 2003 and February 2010. The new regional basin reconstruction method shows that the mass loss within the southeastern basins in the GS has slowed down since 2007, while mass loss in western basins increased showing a progression to the north of Greenland.

Citation: Schrama, E. J. O., and B. Wouters (2011), Revisiting Greenland ice sheet mass loss observed by GRACE, *J. Geophys. Res.*, 116, B02407, doi:10.1029/2009JB006847.

1. Introduction

[2] Monthly gravity fields observed by the Gravity Recovery and Climate Experiment (GRACE) mission, launched in March 2002 [cf. Tapley *et al.*, 2004], suggest that the Greenland system (GS) experiences a significant mass loss. Initially, the Greenland mass loss was identified by Velicogna and Wahr [2005], who found a mean rate of -75 ± 26 Gt/yr between the summers of 2002 and 2004. The method used by Velicogna and Wahr [2005] convolves monthly average mass fields observed by GRACE using the local averaging kernel method of Swenson *et al.* [2003] in which a minimum is sought between the combined measurement error and the signal leakage error.

[3] According to Velicogna and Wahr [2006], GRACE observed -148 ± 22 Gt/yr and -76 ± 17 Gt/yr for south and north Greenland, respectively, while the total GS mass balance is -220 ± 11 Gt/yr between April 2002 and April 2006. Furthermore, Velicogna and Wahr [2006] find that there is an acceleration in the mass loss since the summer of 2004; Greenland was modeled as two separate basins, and individual mass time series are shown for north and south Greenland. It should be noted that Velicogna and Wahr [2005, 2006] rely on the first generation release of the GRACE data which yield consistently less mass loss for the

GS compared to their more recent releases [see also Chen *et al.*, 2006]. In the work by Velicogna [2009] the GS mass loss increased from -137 Gt/yr in 2002–2003 to -286 Gt/yr in 2007–2009. This suggests an acceleration of -30 ± 11 Gt/yr² between 2002 and 2009.

[4] Luthcke *et al.* [2006] estimated the Greenland's ice sheet mass loss to be -101 ± 16 Gt/yr in 2003–2005, more recent estimates for the GS trend presented at the European Geosciences Union (EGU) 2010 meeting mentions -177 ± 6 Gt/yr for August 2003 to August 2009 [see also Luthcke *et al.*, 2010]. The method used by Luthcke *et al.* [2006] is based on a regional mass concentration (hereafter referred to as mascon) solution strategy developed at the Goddard Space Flight Center which fundamentally differs from the solutions presented by Velicogna and Wahr [2005, 2006] and Velicogna [2009] which depend on the monthly spherical harmonic coefficient sets. The difference between the GS mass loss rates reported by Luthcke *et al.* [2006, 2010] and those reported by Velicogna and Wahr [2006] and Velicogna [2009] is significant even if we allow for the acceleration of mass loss.

[5] Wouters *et al.* [2008] estimated Greenland's mass change at -179 ± 25 Gt/yr for 2003–2008, which differs from the results obtained with the averaging kernel method used by Velicogna [2009]. The method of Wouters *et al.* [2008] can be viewed as a posteriori fitting of regional mascons to the global GRACE solutions derived from monthly sets of spherical harmonic coefficients; it is based on a multibasin forward method where Greenland was divided in eight compartments which were each subdivided in a part below and a part above 2000 m following the

¹Faculty of Aerospace Engineering, Delft University of Technology, Delft, Netherlands.

²Koninklijk Nederlands Meteorologisch Instituut, De Bilt, Netherlands.

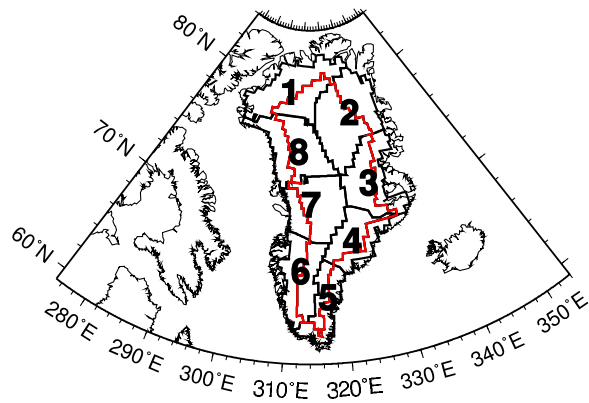


Figure 1. Basins in the Greenland system. For subbasins below 2000 m we use the basin numbers as indicated, for basins above 2000 m the basin number is incremented by 8. Basins outside the GS are 17, Ellesmere Island; 18, Baffin Island; 19, Iceland; and 20, Svalbard.

definitions of *Zwally et al.* [2005] (see Figure 1). In addition to the 16 basins *Wouters et al.* [2008] define a number of regions near the GS including leakage basins in a greater area around the GS such as Ellesmere Island, Baffin Island, Iceland, and Svalbard (here referred to as the EBIS region).

[6] The conclusion of *Velicogna and Wahr* [2006] that Greenland’s mass loss accelerated around the summer of 2004 is confirmed by *Wouters et al.* [2008]. Nevertheless, the mass loss rates between both studies differs more than the formal error between February 2003 and January 2008; it should be mentioned that the results published by *Velicogna and Wahr* [2006] and *Velicogna* [2009] are systematically larger than those presented by *Wouters et al.* [2008] and *Luthcke et al.* [2006, 2010]. The question is therefore why these differences occur and whether the differences can be explained; this issue is significant because of the averaging kernel method of *Swenson et al.* [2003].

[7] One hypothesis is that the kernel function shown in Figure 1 of *Velicogna and Wahr* [2005] overlaps surrounding regions like Ellesmere Island, Baffin Island, Iceland, whereas *Wouters et al.* [2008] and *Luthcke et al.* [2010] focus on the GS with a mascon approach. Another possibility is that the single-basin scale factor in the averaging kernel method used by *Velicogna and Wahr* [2005] is biased in their estimation process.

[8] The cause for differences in the observed mass loss rates within the GS observed by GRACE is a motivation for writing this paper. We introduce a new implementation of the forward method set out by *Wouters et al.* [2008] to efficiently retrieve monthly mass variations for regional basins in the GS. In order to allow variations of our calculated mass time series per basin we also consider the effect of different basin configurations representing the GS including the EBIS region, and we allow variations in the assumed Gaussian smoothing radii. Furthermore, during preprocessing of the GRACE data we will compensate for glacial isostatic adjustment (GIA) with the help of the Paulson model [cf. *Paulson et al.*, 2007] which is based on the ICE-5G ice history as explained by *Peltier* [2004] with a

viscosity profile adjusted to match the GRACE observations. As an alternative we use *Peltier’s* model which assumes the VM2 viscosity profile and the ICE-5G ice history [cf. *Peltier*, 2004]. In section 4 we comment on a new method to classify the contribution of GIA as explained by *Wu et al.* [2010]. Our processing methods depend on monthly sets of spherical harmonic coefficients describing the Earth’s gravity field for which we use (1) the fourth release of the Center of Space Research at Austin Texas (CSR), (2) the fourth release of the GeoForschungsZentrum (GFZ)-Potsdam, Germany, and (3) the ITG-Grace2010 solution developed at the Institut für Geodäsie und Geoinformation in Bonn, Germany [see also *Kurtenbach et al.*, 2009; *Mayer-Gürr*, 2006].

[9] Section 2 introduces a deconvolution method to estimate mass time series for a system represented up to 20 basins taken from *Wouters et al.* [2008] (see Figure 1). In section 3 we apply this method to the investigation of the attenuation affect which occurs when the GS is underrepresented by a single basin rather than several smaller basins which are better able to focus on the source signal in the GS. We also discuss the dependency between the GS solution, basins representing the EBIS region, and the area on Greenland above 2000 m. Furthermore, in section 3 we also show the effect of variations in a Gaussian smoothing radius. In section 4 we discuss the observed acceleration of the surface mass signal, and the conclusions are summarized in section 5.

2. Basin Estimation Method

[10] We assume that a surface mass observation system with infinite resolving power (or angular resolution) provides spatially uncorrelated surface mass data here expressed as water thickness maps. Furthermore, we assume that there are N unit basin functions (i.e., compartments which are filled with 1 m of equivalent water inside their domain). In this situation a monthly surface mass map y_t is approximated by

$$y_t(x) = \sum_{j=1}^N \alpha_{tj} b_j(x) + \epsilon_t(x) \quad \forall x \in \Omega \quad (1)$$

where x is the geographical location at time index t in the GRACE monthly series, $b_j(x)$ is the j th basin function, α_{tj} are uniform scaling factors which are to be determined, and $\epsilon_t(x)$ represents a misfit because we do not expect that N (where N is at most 20) basin functions can precisely describe the observed signal within the model domain Ω . The surface mass signal in y is affected by observation noise and possibly systematic effects, but at infinite angular resolution we assume that a Dirac delta function acts on geographical source signals in y . Once the coefficients α_{tj} are known, the volume for each basin j is determined at time step t . To obtain the mass M_{tj} within basin j at epoch t , we multiply $\alpha_{tj} b_j(x)$ times the density ρ and the area μ_j so that $M_{tj}(x) = \rho \mu_j \alpha_{tj} b_j(x)$.

[11] For the GRACE equivalent water height maps we modify equation (1) because the monthly water thickness data are provided at finite angular resolution. In this paper, equivalent water height grids are computed with a known

Gaussian smoothing function with radius τ truncated at spherical harmonic degree 60, as is explained by, for instance, *Swenson et al.* [2003] and *Schrama et al.* [2007]. This means that the provided GRACE maps should be represented as $z_t(x) = G(y_t(x), \tau)$, where G is the Gaussian convolution operator acting on $y_t(x)$. Since G is an integral over the sphere we can rewrite equation (1) as

$$\begin{aligned} z_t(x) &= \sum_{j=1}^N \alpha_{ij} G(b_j(x), \tau) + G(\epsilon_t(x), \tau) \\ &= \sum_{j=1}^N \alpha_{ij} \beta_j(x) + \gamma_t(x) \end{aligned} \quad (2)$$

where $\beta_j(x)$ is the j th modified basin function which appears when the j th unit basin function $b_j(x)$ is convolved with a Gaussian smoothing operator. Solving equation (2) is the essence of a basin mass reconstruction method where we attempt to determine the coefficients α_{ij} assuming that $z_t(x)$ is provided by a finite angular resolution surface mass observation system such as GRACE.

2.1. GRACE Data Preprocessing and EOF Filtering

[12] Grids of water thickness for month t are contained in z_t in equation (2). The water thickness grid computation as in the work by *Schrama et al.* [2007] relies on empirical orthogonal function (EOF) editing and approximation. This means that a singular value decomposition is applied to a data matrix D so that

$$D = U\Lambda V^T \quad (3)$$

where the diagonal entries of Λ contain so-called singular values which are the square roots of the eigenvalues of the covariance matrices DD^T and $D^T D$. Also, U and V are unitary matrices with eigenvectors of DD^T and $D^T D$, respectively. D contains column wise monthly solutions of the equivalent water heights derived from the provided spherical harmonic coefficients sets relative to an average derived from that set which are convoluted with a Gaussian smoothing operator with radius τ .

[13] GRACE does not observe variations of the geocenter, and observations of C_{20} by GRACE are noisy. As a result, during the processing of the GRACE data we exclude contributions from the geocenter, and we also assume that C_{20} variations are caused by postglacial rebound. Our decision not to correct for a geocenter motion causes our trends for the GS to be underestimated by 8 Gt/yr which is relevant when the results are compared with other methods such as that of *Velicogna* [2009], which is reported in section 4.

[14] In equation (3) the spatial representation of EOF mode i appears in column U_i while its temporal representation is in column V_i . Also, a diagonal entry i in Λ allows determination of the percentage of variance of EOF mode i relative to the total variance.

[15] The EOF method is convenient for identifying “enigmatic” elements in the monthly coefficient sets which we encountered in all solutions obtained from the ITG, the CSR, and the GFZ. A noisy subset within D will typically cause a spike in a dominant EOF V mode. Typically, $k = 10$

EOF modes of D describe more than 80% of its variance; these EOFs are considered to be describing the “dominating directions” of the covariance matrices $D^T D$ and DD^T . Spikes in the first k EOF V modes are associated with noisy months which occur for all provided monthly GRACE gravity field series. By removal of enigmatic months (referred to as EOF editing) we rejected for all GRACE gravity field series all data in 2002; January and February in 2003; and January 2004. For the GFZ and ITG series we edited June 2003 and August–October 2004, and for the ITG solution May 2003 was excluded.

[16] For the monthly gravity coefficient sets that remain we assume an additional EOF compression so that D is approximated by the first k EOF modes associated with the largest singular values. The approximation of D is called $D^\# = U\Lambda^\# V^T$, where $\Lambda^\#$ contains the k largest singular values of Λ , while the remaining diagonal entries are set to zero. More details on the EOF modes of GRACE are explained by *Schrama et al.* [2007]; here we used $k = 10$ which we found adequate to approximate D .

2.2. Numerical Solution of the Basin-Scale Parameters

[17] By solving the α_{ij} coefficients in equation (2) we deconvolve the GRACE water thickness observation as a mass signal in predefined basins. We rescale the problem by estimating $\alpha'_{ij} = \alpha_{ij}/(\rho\mu_j)$ while using $\beta'_j(x) = \rho\mu_j\beta_j(x)$ so that the α'_{ij} parameters represent the aggregated mass values at epoch t for basin j .

[18] The forward method of *Wouters et al.* [2008] solves equation (2) by iterative adjustments of the α_{ij} parameters to minimize the integral of $\gamma_t^2(x)$ within Ω . With this method a limited number cases could be realistically studied because of the computational efficiency of the search procedure converging to an approximate minimum.

[19] Since the present study requires several basin configurations to be investigated, we optimized the forward method by globally minimizing the integrals of $\gamma_t^2(x)$. In order to find an exact least squares minimum we rewrite equation (2) in vector form:

$$\vec{z}_t = [\vec{\beta}'_1 \dots \vec{\beta}'_N] \vec{\alpha}'_t + \vec{\gamma}_t = A \vec{\alpha}'_t + \vec{\gamma}_t \quad (4)$$

and we minimize $\vec{\gamma}_t^T \sigma^{-1} I \vec{\gamma}_t$ whereby it is assumed that all observations in \vec{z}_t are assigned an observation noise variance σ . An unconstrained solution of equation (2) follows from

$$\hat{\alpha}'_t = (\sigma^{-1} A^T A)^{-1} A^T \sigma^{-1} \vec{z}_t = (A^T A)^{-1} A^T \vec{z}_t = Q \vec{z}_t \quad (5)$$

In some cases we modify equation (5) so that a mass variation in basin j is constrained to an a priori variance ω_j so that

$$\hat{\alpha}'_t = (\sigma^{-1} A^T A + W^{-1})^{-1} A^T \sigma^{-1} \vec{z}_t = Q \vec{z}_t \quad (6)$$

where $W_{jj} = 1/\omega_j$ is a diagonal element of W .

[20] The following are some properties of equation (6).

[21] 1. Any monthly input grid \vec{z}_t input to equation (6) contains GRACE equivalent water heights which were computed with a Gaussian smoothing radius τ . Any monthly grid is first multiplied by the corresponding modified basin functions $\beta'_j(x) \forall j \in [1, N]$. This step guarantees that the

algorithm is not significantly affected by signal and noise at distances exceeding twice the assumed Gaussian smoothing radius (τ) relative to the periphery of basin j . Far-field leakage is studied by means of simulations and is found to be negligible except for the contribution of the EBIS regions as explained in Appendix A of *Wouters* [2010].

[22] 2. The efficiency of the algorithm is of order $N \times N_{obs}$ where N_{obs} is the number of provided grid points. The Q matrix in equation (6) is computed in advance; this is a one-time operation with an efficiency of the order N^3 , where N never exceeds 20 for cases that we considered.

[23] 3. The estimated basin scaling coefficients $\hat{\alpha}'$ that result from equation (5) or (6) between adjacent basins are usually found to have a negative correlation. This can be observed by inspecting the covariance matrices of the estimated parameters ($P = (\sigma^{-1}A^T A)^{-1}$ or $P = (\sigma^{-1}A^T A + W^{-1})^{-1}$ depending on the choice of the algorithm.) The consequence of negative correlations is that aggregate mass time series over a number of adjacent basins become less noisy than mass time series for individual basins. For this reason we can decide to include a priori constraints indicated by the W matrix in equation (6) for basin configurations that are explained in more detail in section 3. A typical a priori constraint could be to restrict the allowed mass variation by basin depending on its physical properties; that is, basins representing an ocean area or surface mass variations above 2000 m in the GS should receive less variance after the least squares update compared with basins located in the coastal zone of the GS.

[24] We comment on the use of constraint equations in sections 3 and 4.

3. Results Obtained With the Basin Mass Estimation Method

[25] Section 3.1 describes the mass time series for the GS and a separate series for the surrounding regions as discussed in section 2. We also devote attention to the numerical solution of the defocusing problem posed in equation (2) because the numerical stability of equations (5) and (6) depends on the basin configuration. Section 3.2 describes the behavior of the mass time series for individual basins in the GS whose mass variations suggest the presence of an accelerating mass loss as reported by *Velicogna* [2009].

[26] All presented results are based on monthly gravity solutions from the CSR and the GFZ which are retrieved from <ftp://podaac.jpl.nasa.gov/grace>. We also used the ITG-Grace2010 solution which is retrieved from <ftp://skylab.itg.uni-bonn.de/ITG-Grace2010/monthly/ITG-Grace2010/>. The coefficients sets are processed as explained in section 2.1; our data set covers the time period March 2003 to February 2010 for the CSR release 4 solution, the ITG-Grace2010 solution ends in August 2009 and the GFZ release 4 solution in January 2010.

3.1. Aggregated Mass Time Series

[27] Since our results depend on the setup of basins in the model domain, we consider basin configurations consisting of (1) one basin which is the overlap of basins 1 to 16 as in Figure 1, (2) eight basins representing the GS coastal zone,

i.e., basins 1 to 8, (3) nine basins where basins 1 to 8 are representing the coastal zone including one common basin that overlaps basins 9 to 16, (4) 13 basins which is the 9-basin configuration where we included four basins in the EBIS region, (5) 16 basins which are basins 1 to 16 as in Figure 1, and (6) 20 basins which is the 16-basin configuration where we included four basins in the EBIS region.

[28] For each basin configuration we solved equation (6) under the assumption that the entries on the diagonal of W , the so-called a priori variance for the basin masses, are greater than 10^6 Gt². In this way we obtain virtually unconstrained solutions for a basin configuration because the results of this setup are close to a so-called Moore-Penrose pseudoinverse of the least squares problem as in equation (5) (for details, see *Stoer and Bulirsch* [2003]). The aggregated mass time signal formed as a sum over all basins in the solution is assumed to be unaffected by internal correlations when W is modeled as αI where $\alpha = 10^6$ Gt².

[29] The normal equations that appear in equation (6) appear with friendly numerical condition numbers for all mentioned configurations, i.e., the condition numbers are 21.9, 40.7, 44.8, 7605, and 7823 for configurations consisting of 8, 9, 13, 16 and 20 basins, respectively. This suggests that no more than 4 significant digits vanish in the calculation of the inverse of the normal equations, albeit that it helps for numerical stability to merge basins 9 to 16 in Figure 1 into a single basin.

[30] The obtained solutions of the aggregated mass time signal are subjected to a separate least squares regression analysis of which the results are shown in Table 1 for configurations consisting of 1, 8, 16 and 20 basins. The obtained regression parameters include trend, acceleration, and annual terms, while the reference time is at the start of 2006. Table 1 shows the single-basin configurations for the GS, the aggregated signal over eight coastal basins excluding the area over 2000 m, the aggregated signal over eight coastal basins and eight basins over 2000 m, and the 20-basin contribution of the GS and EBIS.

[31] From the results in Table 1 we conclude that basin representation choice by either one or more basins is more significant than any other control parameter used in Table 1, such as the choice of a gravity coefficient set or the employed GIA correction models. All single-basin results (Table 1, single basin) provide a strong indication that the estimated mass signal is significantly attenuated. This can be seen when the obtained regression parameters are compared with the eight coastal basin configuration results as displayed in Table 1 (8 basin).

[32] Our conclusion from Table 1 is that the GS mass loss rates are on average -145.9 ± 13.4 Gt/yr (95% confidence intervals are shown in this paper) when the GS is represented by a single basin, and it becomes -207.1 ± 18.2 Gt/yr when the GS is represented by eight smaller coastal basins; the attenuation (defined as the difference divided by the largest surface mass rate times 100%) is 29.6%. A second indication that the GS is better represented by eight basins than one single basin which follows from the measure of success of an approach, S , which we define as $S = (1 - (\sigma_2/\sigma_1)^2) \times 100\%$, i.e., the ratio between the variances of the observed minus model difference (σ_2^2) and the variance of the observations (σ_1^2) of a solution within a restricted domain

Table 1. Greenland System Mass Change Regression Parameters Modeled in 1, 8, 16, or 20 Basins^a

Center	GIA	Rate	Accel	H	G	σ_1	σ_2	σ_3
<i>Single-Basin Configurations</i>								
CSR	Paulson	-154.7	-15.8	30.7	130.1	7.25	6.25	25.07
CSR	VM2	-145.8	-15.6	30.9	130.7	6.86	6.27	25.37
GFZ	Paulson	-140.5	-17.4	39.2	147.0	6.64	5.64	27.15
GFZ	VM2	-136.4	-16.4	38.5	146.2	6.43	5.68	26.56
ITG	Paulson	-151.1	-12.6	35.6	149.9	6.25	5.59	21.84
ITG	VM2	-146.8	-11.8	35.1	148.6	6.06	5.68	19.72
<i>Eight-Basin Configurations</i>								
CSR	Paulson	-217.0	-13.5	53.6	132.1	9.07	3.31	35.51
CSR	VM2	-208.8	-13.3	53.9	132.6	8.83	3.15	36.01
GFZ	Paulson	-196.9	-16.8	66.4	145.7	8.27	3.02	35.07
GFZ	VM2	-194.9	-15.3	65.4	145.0	8.17	2.86	34.00
ITG	Paulson	-213.7	-11.6	64.7	147.6	7.98	2.82	30.24
ITG	VM2	-211.3	-10.4	64.0	146.6	7.92	2.69	27.00
<i>Sixteen-Basin Configurations</i>								
CSR	Paulson	-228.1	-15.5	54.7	165.4	9.36	2.65	42.98
CSR	VM2	-218.7	-15.4	55.2	165.7	9.09	2.52	43.39
GFZ	Paulson	-208.2	-21.9	73.6	171.1	8.55	2.36	40.86
GFZ	VM2	-207.0	-20.3	72.2	170.8	8.43	2.24	40.32
ITG	Paulson	-227.3	-13.4	70.1	171.3	8.22	2.25	32.82
ITG	VM2	-225.7	-12.2	68.9	170.6	8.14	2.15	29.73
<i>Twenty-Basin Configurations</i>								
CSR	Paulson	-267.2	-20.4	82.9	190.1	9.32	1.99	64.33
CSR	VM2	-251.1	-20.2	83.6	190.1	9.06	1.99	64.56
GFZ	Paulson	-242.2	-26.8	113.7	188.4	8.47	1.86	53.28
GFZ	VM2	-228.1	-24.9	112.0	188.4	8.35	1.90	52.49
ITG	Paulson	-263.1	-20.2	102.9	192.7	8.20	1.66	47.07
ITG	VM2	-248.6	-18.7	101.4	192.5	8.12	1.71	43.51

^aCenter indicates whether GRACE gravity data are provided by CSR, GFZ, or ITG; GIA refers to the glacial isostatic adjustment models of ICE-5G/Paulson and ICE-5G/VM2; Rate, the mass loss rates in Gt/yr; Accel, the mass loss acceleration; H, the annual amplitude, in Gt; and G, the phase as day of year. The standard deviation of observation residuals, σ_2 , is expressed in cm of water thickness, and the explained signal, σ_1 , in cm of water thickness; both parameters are computed between 285°W and 350°W and 60°N and 86°N. The standard deviation, σ_3 , in Gt of the GS time mass series relative to the regression model. All cases assume a smoothing radius of 3° and 10 EOFs to compress D as in equation (3). Note that single-, 8-, and 16-basin entries refer to the GS, whereas 20-basin entries refer to the GS, including the EBIS region.

around the GS (for details, see Table 1). Single-basin solutions have an average success rate of around 20%, while all eight-basin cases yield around 94%. A third indicator concerns the annual amplitude and phase of the solutions presented in Table 1; the phase of all solutions is relatively stable around day of the year 141.6 ± 14.4 , yet the amplitudes of single-basin solutions are on average 57% compared with those obtained from eight-basin solutions. This scaling factor should not be applied to the observed trends and accelerations where the ratios are on average 70% and 111% between both configurations. Our conclusion is therefore that one cannot simply apply a uniform scale to a single-basin result to predict an eight-basin result in Table 1.

[33] The main conclusion is, however, that a GS mass time series is underrepresented with a single-basin configuration using the method outlined in section 2. The best explanation is that the signal of interest occurs on the flanks of the β_j^i functions [cf. Luthcke et al., 2006; Wouters et al., 2008; van den Broeke et al., 2009]. These basin functions

originate from a unit basin function that is convoluted with a Gaussian smoothing operator. In equation (6) the GRACE-derived equivalent water heights (which are strongest on the flanks of a single basin) are multiplied by the $\beta_j^i(x)$ function. The off-centering between the source signal and the basin function is in our opinion the cause for underestimating the mass signal. This situation is different in the eight-basin configuration where multiplications of the source signal take place more toward the centers of the $\beta_j^i(x)$ functions; this explains why we see larger GS mass loss signals for the eight-basin configuration displayed in Table 1 compared with the single-basin configuration.

3.2. Signal Above 2000 m in the GS and the EBIS Region

[34] In Table 2 we show mass change trends for 16- and 20-basin solutions where the confidence intervals follow from calculations based on three gravity models and two GIA models as used in Table 1. Our conclusion from Table 2 is that a larger mass loss rate results from the defocusing method when we add the EBIS region to the solution in which case we see a change from -219.2 ± 19.1 Gt/yr to -250.1 ± 28.4 Gt/yr. The difference between both mass loss rates should, however, not be interpreted in the sense that the increased mass loss only originates from the EBIS region. Instead, we see that by adding the EBIS region to the model domain that mass changes are distributed within the system. We will comment on the interpretation of these results in section 4.

[35] The normal equations in (6) show “friendly” condition numbers, but there are noticeable negative correlations between adjacent basins. The condition number of the 9-basin solution is 40.7 which is a significant improvement compared to 7605 for the 16-basin solution, meaning that it helps to combine basins 9 to 16 above 2000 m in the GS into a single basin.

[36] Configurations consisting of 9, 13, 16, and 20 basins all show significant negative correlations between the aggregated signal from basins below and above 2000 m. For a nine-basin configuration we find a correlation of -0.89 which follows from the formal error covariance matrix P of the parameters (see equation (6)). In a similar way we find for the 16-basin configuration a correlation coefficient of -0.975 . In this context, correlation coefficients directly follow from the product $\vec{v}^T P \vec{v}$ where \vec{v} is a suitably designed matrix consisting of two or three column vectors and P is the inverse of the normal equations following from equation (6). As a result, of the negative correlations that

Table 2. Mass Change Trends in the Model Domain^a

Area	16 Basins	20 Basins
GS	-219.2 ± 19.1	-201.4 ± 21.0
GS under 2000 m	-322.3 ± 53.3	-263.3 ± 55.6
GS above 2000 m	103.1 ± 44.0	62.0 ± 46.5
EBIS		-48.7 ± 18.0
GS + EBIS		-250.1 ± 28.4

^aArea refers the Greenland system (GS) or the surrounding regions, Ellesmere island, Baffin island, Iceland, and Svalbard (EBIS). Solutions are obtained for 16 and 20 basins (see also section 3.2). All mass change trends are in Gt/yr including a 95% probability window.

Table 3. Mass Change Regression Parameters Obtained From an Unconstrained Configuration of 13 Basins Presenting the Greenland System and Four Surrounding Regions^a

Basin or Area	Gt/yr	Gt/yr ²	H	G
Basin 1	-18.6 ± 5.4	-1.6 ± 2.0	7.7 ± 3.4	212.6 ± 24.4
Basin 2	-7.2 ± 5.5	-2.4 ± 8.1	13.3 ± 5.3	216.4 ± 22.0
Basin 3	-33.5 ± 6.4	6.4 ± 9.9	19.1 ± 6.9	179.7 ± 25.9
Basin 4	-52.4 ± 6.2	8.8 ± 1.0	17.2 ± 10.7	123.7 ± 38.3
Basin 5	-56.7 ± 10.1	4.3 ± 0.9	17.5 ± 15.7	152.7 ± 34.8
Basin 6	-5.6 ± 11.0	-9.0 ± 1.4	23.8 ± 4.9	107.7 ± 17.6
Basin 7	-32.5 ± 2.8	-3.3 ± 2.6	11.6 ± 5.4	204.6 ± 20.3
Basin 8	-43.2 ± 6.1	-13.1 ± 3.2	2.3 ± 4.7	129.8 ± 135.2
Ellesmere Island	-21.9 ± 6.6	-11.5 ± 2.3	29.2 ± 4.5	239.7 ± 7.6
Baffin Island	-10.8 ± 15.2	-12.4 ± 7.1	26.4 ± 5.1	122.2 ± 14.9
Iceland	-12.7 ± 4.9	3.1 ± 5.1	13.9 ± 4.7	256.8 ± 17.1
Svalbard	-5.4 ± 2.6	7.4 ± 1.0	36.2 ± 4.8	246.1 ± 12.7
Greenland	-201.1 ± 18.7	-8.3 ± 6.5	64.5 ± 9.9	133.1 ± 9.2
GS below 2000 m	-249.7 ± 20.4	-9.9 ± 16.9	86.9 ± 16.5	159.6 ± 8.8
GS above 2000 m	+48.6 ± 9.6	1.5 ± 11.1	40.6 ± 25.9	22.0 ± 21.8
EBIS region	-50.8 ± 17.3	-13.4 ± 3.3	68.8 ± 10.2	226.2 ± 8.7
Full system	-251.9 ± 28.2	-21.8 ± 3.6	92.8 ± 22.0	181.6 ± 6.3

^aThese results are obtained from all available GIA models and GRACE solutions assuming a 3° smoothing radius. The basin rates and accelerations are calculated relative to the start of 2006, annual amplitudes for H are expressed in Gt, while the phase is represented as day of year for G . For all regression parameters we show a 95% confidence region.

occur in $\vec{v}^T P \vec{v}$ we conclude that it is difficult to uncouple signals above and below 2000 m. Yet the conclusion is also that the total mass change over the GS is better determined than the individual summed signals above and below 2000 m (see also Table 2).

[37] We consider a 13-basin configuration where the area in the GS above 2000 m is represented by one basin. The condition number of the 13-basin solution is 44.8 which is a significant improvement compared to a condition number of 7823 of a 20-basin solution. We conclude that mass loss rates shown for the 13-basin solution in Table 3 are not significantly different compared with the 20-basin configuration in Table 2; that is, the differences occur within the indicated confidence regions; also, the confidence region of any 13-basin solution is significantly improved compared with a 20-basin solution. For the correlation coefficients that occur below and above 2000 m in the GS we find -0.89 for 13-basin solutions and -0.97 for 20-basin solutions. The remaining error correlation coefficients in the system are between -0.26 and 0.21.

[38] Our conclusion is that the configuration of 13 basins can be used for studying the system. For this configuration in Table 3 we show the solved-for regression parameters trend, acceleration, annual amplitude, and phase both in aggregated form and also by defined basin within the model domain. All values in Table 3 are obtained for a 3 degree smoothing radius and a 13-basin configuration where two GIA models and three gravity solutions are used. The conclusion from the 13-basin model is that (1) most of the mass loss originates from the coastal zone where we observe -249.7 ± 20.4 Gt/yr, (2) the area above 2000 m in the GS is gaining mass by 48.6 ± 9.6 Gt/yr, (3) the uncertainty in this signal is correlated by -0.89 to an uncertainty in the coastal region mass signal, (4) the EBIS region is losing mass at a rate of -50.8 ± 17.3 Gt/yr,

and (5) uncertainties in the latter signal are correlated by -0.25 to coastal zone and by +0.19 to the area above 2000 m in the GS.

[39] *Wouters et al.* [2008] described a solution that was not obtained by formally solving the normal equations, instead with the method of *Wouters et al.* [2008] one calculates a signal correlation between different basins, but this is fundamentally another quantity than a formal error correlation as derived from the inverse of the normal equations stored in matrix P . A more recent implementation of the method described by *Wouters et al.* [2008] shows for the GS a mass gain of 37 ± 15 Gt/yr above 2000 m, a mass loss of -244 ± 14 Gt/yr below 2000 m, resulting in a total mass loss of -207 ± 22 Gt/yr between March 2003 and February 2010. The mascon solution presented by *Luthcke et al.* [2010] mentions 65 ± 9 Gt/yr above 2000 m and -242 ± 19 Gt/yr in the coastal zone of the GS between August 2003 and July 2009. We will comment on the significance of a mass gain signal above 2000 m in section 4.

3.3. Influence of the Smoothing Radius

[40] All results discussed in sections 3.1 and 3.2 were computed with a smoothing radius of 3°. The choice of a smoothing radius leaves a degree of arbitrariness in the results, although *Schrama et al.* [2007] obtained an optimal fit with external GPS data for a radius of 4 degrees. Due to the fact that the GS is situated at more northern latitudes where the GRACE tracks converge and also because the latest edited data sets from GRACE include up to 82 months, we are able to shorten the smoothing radius to 2.5 degrees. To assess the effect of the smoothing radius, we consider that radii may be varied between 2.5 and 3.5 degrees in steps of 0.5 degree.

[41] For the 13-basin solution we find that the average mass loss rate of the GS becomes -199.8 ± 19.8 Gt/yr with an acceleration of -8.8 ± 6.3 Gt/yr². For the annual amplitude we find 64.6 ± 16.0 Gt and a phase at day of year 132.0 ± 14.1 . We notice that there are no significant changes in the mean values of the obtained trend parameters compared to a calculation where we fix the smoothing radius at 3°, except that the confidence region tends to increase; that is, for $\tau = 3^\circ$ we obtain an average mass loss rate of the GS at -201.1 ± 18.7 Gt/yr and an acceleration of -8.3 ± 6.5 Gt/yr² an amplitude of 64.5 ± 9.9 Gt and a phase at day of year 133.1 ± 9.2 .

4. Discussion

[42] The GS mass loss represented as an ensemble average and its 95% probability region based on all used analysis centers with consideration of variations in the smoothing radius, GIA models, and different GRACE processing centers as described in sections 2 and 3 is shown in Figure 2, which follows from a configuration of 13 basins. Figure 2 is dominated by mass losses in the coastal zone which is independently confirmed by ICESat altimetry data analysis as in, for instance, the work by *Slobbe et al.* [2009] but also by *Pritchard et al.* [2009].

[43] The analysis underlying the results in Tables 2 and 3 shows that mass change error variances in the area above and below 2000 m in the GS are significantly anticorrelated while error variances in the EBIS region are weakly coupled

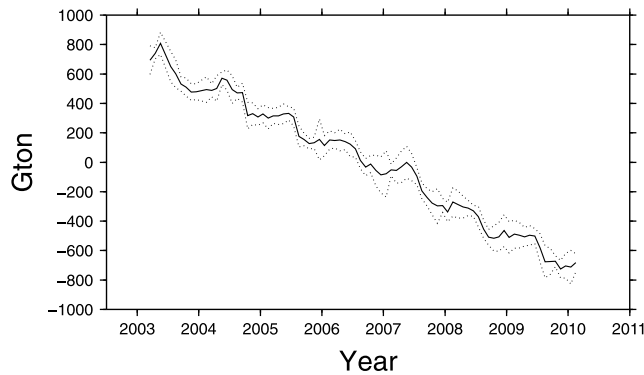


Figure 2. Evolution of the average mass in Gt aggregated over basins in the Greenland system based on a configuration consisting of 13 basins. The average and a 95% probability region follow from variations in the smoothing radius, the GIA correction models of ICE-5G/Paulson and ICE-5G/VM2, and the selection of CSR, GFZ, and ITG monthly spherical harmonic coefficient series.

to the GS (see also section 3.2). Independent constraints on the GS mass signal above 2000 m may be derived from ice topography profiles observed by the laser altimeter on ICESat. This suggests a thickening of Greenland as reported by Pritchard *et al.* [2009]. However, ICESat provides a volume measurement and not a mass measurement, and a conversion from volume to mass measurements requires knowledge of the density of the ice sheet's firm layer, which is spatially and temporally variable due to variations in accumulation in temperatures [see also Helsen *et al.*, 2008]. Furthermore, ICESat cannot observe the percolation and refreezing of glacial meltwater that flows through crevasses in the Greenland ice sheet. In our opinion a more realistic independent constraint on the signal above 2000 m should come from the surface mass balance calculation as shown by van den Broeke *et al.* [2009].

[44] We find that the GS and EBIS are experiencing a statistically significant acceleration which agrees with the conclusion of Velicogna [2009]. However, our computed acceleration of -8.3 ± 6.5 Gt/yr² for the GS alone is less than the value of -30 ± 11 Gt/yr² published by Velicogna [2009]. A better agreement is found when we include the EBIS region in our calculations in which case we find for the entire system an acceleration of -21.8 ± 3.6 Gt/yr².

[45] One of the possible causes why our mass loss trends differ from the results published by Velicogna [2009] is that they used GRACE data in 2002 which we did not consider; furthermore, we used all GRACE data in 2009 including January and February of 2010, which show an above average mass accumulation. The presence of an acceleration term is certainly one of the reasons why different surface mass trend values for the GS can be obtained from the GRACE mission data analysis. However, we remark that the short time series and the large interannual variability of the GS as described by Ettema *et al.* [2009] affects the physical significance of the obtained acceleration values.

[46] We suggest that the observed mass loss in the EBIS region could be responsible for different values published by

Table 4. GRACE Observed Seasonal Mass Changes Between March 2003 and February 2010^a

	Jan-Mar	Apr-Jun	Jul-Sep	Oct-Dec
2003		80.1	-179.8	-104.8
2004	2.3	51.9	-64.4	-160.9
2005	-3.8	11.0	-112.3	-75.0
2006	-0.4	-0.0	-114.0	-75.2
2007	-10.7	40.5	-154.5	-113.5
2008	-8.5	-17.1	-129.0	-52.1
2009	-2.1	-3.2	-142.5	-56.7
2010	3.1			
Average	-2.9	23.3	-128.1	-91.2

^aAll values are in Gt constructed from the 13-basin ensemble average shown in Figure 2. Average represents the seasonal averages between 2003 and 2010.

Wouters *et al.* [2008], Luthcke *et al.* [2010], and Velicogna [2009], whose averaging kernel partially overlaps Ellesmere Island. When we use an averaging kernel similar to that of Velicogna and Wahr [2006], we find that due to the overlap a 1 Gt/yr mass change over Ellesmere Island adds up to 0.3–0.5 Gt/yr to the total mass trend estimate of the GS, depending on the location. Baffin Island and Iceland have a much lower impact; here a 1 Gt/yr signal would add 0.1 and 0.05 Gt/yr (for a discussion, see Wouters [2010]).

[47] Table 4 shows the quarterly GRACE observed mass changes between March 2003 and February 2010 where all values are expressed in Gt; Table 4 is constructed from the ensemble average shown in Figure 2. This result suggests that the negative mass balance of Greenland is caused by the fact that the summer and autumn mass loss in any year greatly exceeds the GS mass gain from precipitation during the winter and spring.

[48] A more extensive discussion based on a surface mass balance (SMB) calculation employing a regional climate model for the Greenland ice sheet corrected for glacier discharge values (D) observed by SAR interferometry is given by van den Broeke *et al.* [2009]. Their SMB-D estimate of -237 ± 20 Gt/yr between 2003 and 2008 is independent from GRACE. The discrepancy between a SMB-D value and our estimate of -201.1 ± 18.7 Gt/yr could be reduced if we allow 8 Gt/yr to come from the geocenter variations which are not observed by GRACE [see also

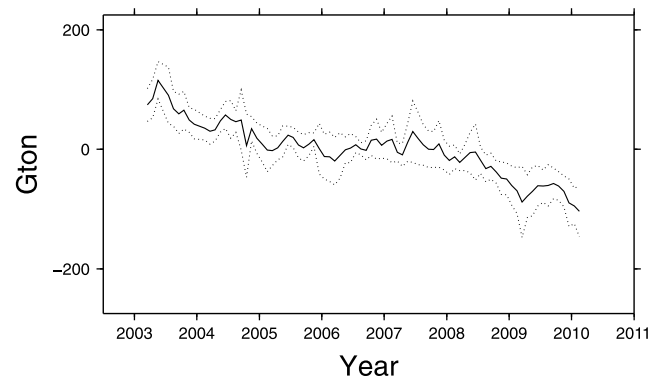


Figure 3. Evolution of mass change in Gt aggregated over basin 1 in north Greenland.

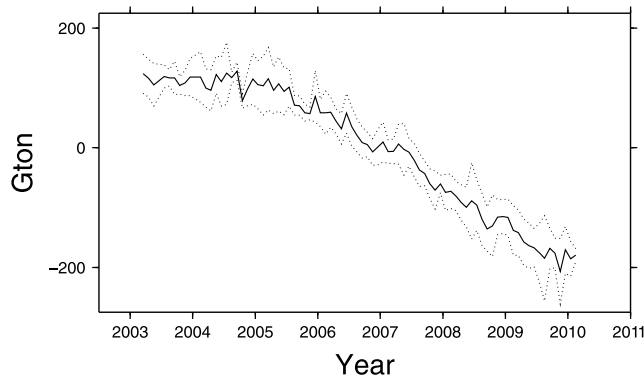


Figure 4. Evolution of mass change in Gt aggregated over basin 8 in northwest Greenland.

Wouters, 2010]. The geocenter correction may also explain the mass loss trend difference that we see compared with that of *Velicogna [2009]*, who did apply a geocenter correction.

[49] The new model developed by *Wu et al. [2010]* provides a new insight into the contribution of postglacial rebound since present-day estimates near Greenland could be affected by a glaciation period that is not part of the ICE-5G model used by *Peltier [2004]* and *Paulson et al. [2007]*. *Wu et al. [2010]* suggested that Greenland shows a present-day mass loss of -104 ± 23 Gt/yr between 2002 and 2008, which is significantly different from any of our GS mass loss estimates with GIA corrections following from the models developed by *Peltier [2004]* and *Paulson et al. [2007]*. The difference of our GS mass loss results compared with those of *Wu et al. [2010]* cannot be explained by the observed acceleration of mass loss in the model domain. In addition, we remark that the new GIA approach of *Wu et al. [2010]* widens the discrepancy between GRACE-derived Greenland mass loss rates and similar results obtained by climatologic studies such as presented by *van den Broeke et al. [2009]*.

[50] A further inspection of mass time series in the GS coastal basins identifies the source basins responsible for a trend change within the analyzed data set. Figures 3, 4, and 5 show mass time series for three selected coastal

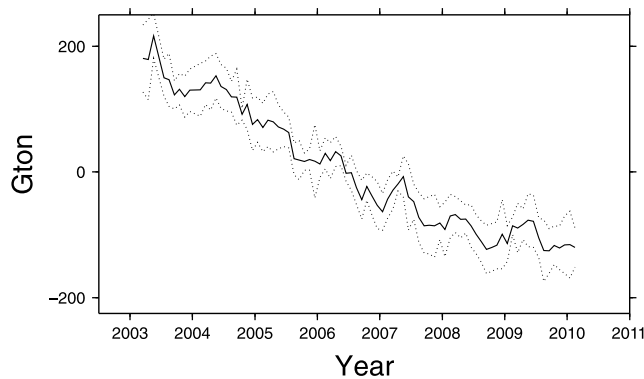


Figure 5. Evolution of average mass in Gt aggregated over basin 4 in southeast Greenland.

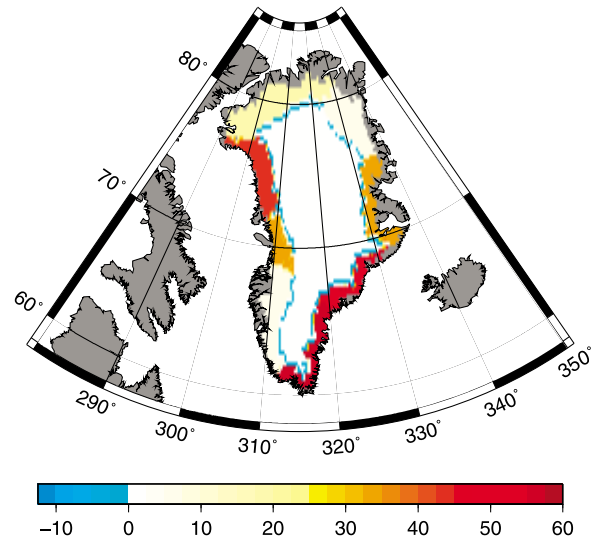


Figure 6. Mass loss rates displayed as the negative trend values shown in Table 3 for coastal basins in the Greenland system.

basins using an ensemble of 13-basin configuration solutions. The signal in basin 1 displayed in Figure 3 shows that north Greenland was stable between 2005 and 2008. The mass change signal in basin 8 is displayed in Figure 4; here we see that the region was stable until the summer of 2005, yet mass loss in basin 8 increased since 2005. Figure 5 shows the opposite behavior; that is, mass loss in basin 4 located in southeast Greenland has slowed down since 2007. This analysis suggests that the GS mass loss is not shifting from the southeast to the north-northwest; in fact, the southeast glaciers are still losing mass, rather the ice mass loss is spreading to the north-northwest. Figure 6 shows the spatial distribution of the GS mass loss in the coastal zone of the GS. The mass loss rates in Figure 6 show that the southeast still dominates between March

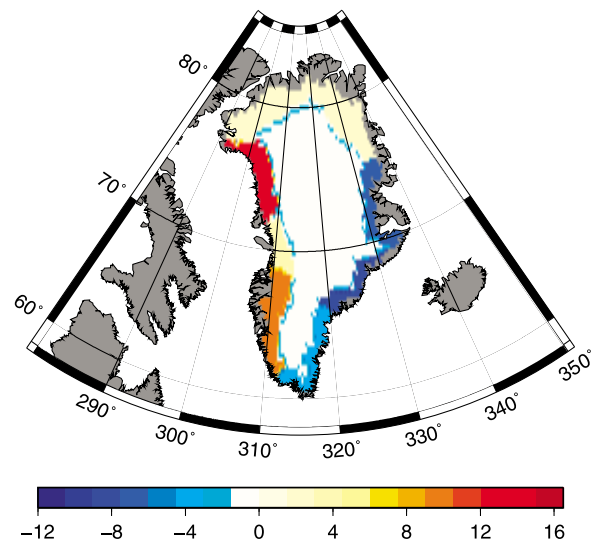


Figure 7. Acceleration of mass change in Gt/yr² for coastal basins in the Greenland system (see also Table 3).

2003 and February 2010, but the accelerations in Figure 7 indicate that the rate of mass loss reduced on the east side of the GS while the western mass loss rates are increasing.

5. Conclusions

[51] The motivation of this paper is to identify spatial and temporal variations in mass loss within in the Greenland system seen by GRACE. To investigate this problem, we developed an optimized forward model to determine mass time series and their error correlations for a configuration of hydrological basins. We use the GRACE level 2 spherical harmonic coefficient sets provided as monthly gravity solutions from the CSR, the GFZ, and the ITG, and we rely on basin definitions as given by *Wouters et al.* [2008] for the GS and calculate mass variations for individual basins. In the analysis we considered the GIA correction models of both ICE-5G/Paulson and ICE-5G/VM2 and a variation in the Gaussian smoothing radii between 2.5 and 3.5 degrees.

[52] With the forward model implemented in this paper, signal attenuation occurs when too few hydrological basins are used to model the mass variations. We tested this hypothesis by modeling the GS as one single basin and, alternatively, as eight coastal basins. The single-basin representation underestimates the GS ablation rate by about 30%, while annual amplitudes are reduced by 43%. Signal attenuation also becomes visible when the standard deviation of model minus the observations and the signal standard deviation of the observations themselves within the model area are compared for different basin configurations. If we assume a 13-basin GS configuration, we find for an ensemble of GRACE-based solutions a mass loss of -201.1 ± 18.7 Gt/yr with an acceleration of -8.3 ± 6.5 Gt/yr² for the time frame March 2003 to February 2010. This result is in agreement with a recent result obtained with the method described by *Wouters et al.* [2008] over the same time frame. Although the total mass loss of the GS is well determined, we find that the GRACE-observed mass changes below and above 2000 m are anticorrelated by -0.89 . In this analysis the area above 2000 m in the GS is represented by a single basin in the defocusing method for which we find a mass gain of 48.6 ± 9.6 Gt/yr.

[53] With the analysis underlying the results presented in Table 3 we find a mass loss of -50.8 ± 17.3 Gt/yr and an acceleration of -13.4 ± 3.3 Gt/yr² over Ellesmere Island, Baffin Island, Iceland, and Svalbard. This finding may explain why *Velicogna* [2009], who used an averaging kernel that partially overlaps Ellesmere Island, finds a systematically larger mass loss rate of -230 ± 33 Gt/yr between 2002 and 2009 when compared with the results of *Wouters et al.* [2008] and *Luthcke et al.* [2010]. The difference between the mass loss value reported by *Velicogna* [2009] and our value of -201.1 ± 18.7 Gt/yr may be reduced by 8 Gt/yr as a result of geocenter variations which are not observed by GRACE.

[54] With our new implementation of the forward method we demonstrate that mass loss trend and acceleration can be identified, whereby it should be mentioned that there is a significant negative error correlation between the summed signal of the coastal basins and the summed mass change signal above 2000 m in the GS. Due to this anticorrelation, internal errors within the GS model domain cancel in the

total mass calculation. Individual coastal basins display unique mass loss patterns; we found that coastal basins in the northwestern and northern part of the GS appear to be affected by a discontinuity in the surface mass loss in 2005 and 2007, while the southeast part of the GS shows a slowdown since 2007.

[55] The relation between the spatial and temporal mass loss pattern in the GS and regional climate models requires a more in-depth study using methodologies such as developed by *van den Broeke et al.* [2009] applied to individual Greenland basins. Our formal error covariance matrix P of the estimated basin mass changes should be considered when such independent results are compared.

[56] **Acknowledgments.** Bert Wouters was funded by the Netherlands Organisation for Scientific research (NWO), GRACE level 2 science data were kindly provided by the Center of Space Research at Austin, Texas; the GeoForschungsZentrum-Potsdam, Germany; and the Institut für Geodäsie und Geoinformation in Bonn, Germany. Jason Box from the Ohio State University, three reviewers, and an Associate Editor provided valuable comments on our manuscript.

References

- Chen, J. L., C. R. Wilson, and B. D. Tapley (2006), Satellite gravity measurements confirm accelerated melting of Greenland ice sheet, *Science*, *313*, 1958–1960, doi:10.1126/science.1129007.
- Ettema, J., M. R. van den Broeke, E. van Meijgaard, W. J. van de Berg, J. L. Bamber, J. E. Box, and R. C. Bales (2009), Higher surface mass balance of the Greenland ice sheet revealed by high-resolution climate modeling, *Geophys. Res. Lett.*, *36*, L12501, doi:10.1029/2009GL038110.
- Helsen, M. M., M. R. van den Broeke, R. S. W. van de Wal, W. J. van de Berg, E. van Meijgaard, C. H. Davis, Y. Li, and I. Goodwin (2008), Elevation changes in Antarctica mainly determined by accumulation variability, *Science*, *320*(5883), 1626–1629, doi:10.1126/science.1153894.
- Kurtenbach, E., T. Mayer-Gürr, and A. Eicker, (2009), Deriving daily snapshots of the Earth's gravity field from GRACE L1B data using Kalman filtering, *Geophys. Res. Lett.*, *36*, L17102, doi:10.1029/2009GL039564.
- Luthcke, S. B., H. J. Zwally, W. Abdalati, D. D. Rowlands, R. D. Ray, R. S. Nerem, F. G. Lemoine, J. J. McCarthy, and D. S. Chinn (2006), Recent Greenland ice mass loss by drainage system from satellite gravity observations, *Science*, *314*, 1286–1289, doi:10.1126/science.1130776.
- Luthcke, S. B., J. J. McCarthy, D. D. Rowlands, A. Arendt, T. Sabaka, J. P. Boy, and F. G. Lemoine (2010), Observing changes in the Land Ice from GRACE and Future Spaceborne Multi-Beam Laser Altimeters, paper EGU2010-5576 presented at EGU Conference, Vienna, Austria.
- Mayer-Gürr, T. (2006), Gravitationsfeldbestimmung aus der Analyse kurzer Bahnboegen am Beispiel der Satellitenmissionen CHAMP und GRACE, Ph.D. dissertation, Univ. of Bonn, Bonn, Germany.
- Paulson, A., S. Zhong, and J. Wahr (2007), Inference of mantle viscosity from GRACE and relative sea level data, *Geophys. J. Int.*, *171*, 497–508, doi:10.1111/j.1365-246X.2007.03556.x.
- Peltier, W. R. (2004), Global glacial isostasy and the surface of the ice-age Earth: The ICE-5G (VM2) model and GRACE, *Annu. Rev. Earth Planet. Sci.*, *32*, 111–149, doi:10.1146/annurev.earth.32.082503.144359.
- Pritchard, H. D., R. J. Arthern, D. G. Vaughan, and L. A. Edwards (2009), Extensive dynamic thinning on the margins of the Greenland and Antarctic ice sheets, *Nature*, *461*, 971–975, doi:10.1038/nature08471.
- Schrma, E. J. O., B. Wouters, and D. A. Lavallée (2007), Signal and noise in Gravity Recovery and Climate Experiment (GRACE) observed surface mass variations, *J. Geophys. Res.*, *112*, B08407, doi:10.1029/2006JB004882.
- Slobbe, D. C., P. Ditmar, and R. C. Lindenbergh (2009), Estimating the rates of mass change, ice volume change and snow volume change in Greenland from ICESat and GRACE data, *Geophys. J. Int.*, *176*, 95–106, doi:10.1111/j.1365-246X.2008.03978.x.
- Stoer, J., and R. Bulirsch (2003), *Introduction to Numerical Analysis, Texts Appl. Math.*, vol. 12, Springer, Berlin.
- Swenson, S., J. Wahr, and P. C. D. Milly (2003), Estimated accuracies of regional water storage variations inferred from the Gravity Recovery and Climate Experiment (GRACE), *Water Resour. Res.*, *39*(8), 1223, doi:10.1029/2002WR001808.

- Tapley, B. D., S. Bettadpur, M. Watkins, and C. Reigber (2004), The gravity recovery and climate experiment: Mission overview and early results, *Geophys. Res. Lett.*, *31*, L09607, doi:10.1029/2004GL019920.
- van den Broeke, M., J. Bamber, J. Ettema, E. Rignot, E. Schrama, W. J. van de Berg, E. van Meijgaard, I. Velicogna, and B. Wouters (2009), Partitioning of Greenland mass loss, *Science*, *326*, 984–986, doi:10.1126/science.1178176.
- Velicogna, I. (2009), Increasing rates of ice mass loss from the Greenland and Antarctic ice sheets revealed by GRACE, *Geophys. Res. Lett.*, *36*, L19503, doi:10.1029/2009GL040222.
- Velicogna, I., and J. Wahr (2005), Greenland mass balance from GRACE, *Geophys. Res. Lett.*, *32*, L18505, doi:10.1029/2005GL023955.
- Velicogna, I., and J. Wahr (2006), Acceleration of Greenland ice mass loss in spring 2004, *Nature*, *443*, 329–331, doi:10.1038/nature05168.
- Wouters, B. (2010) Identification and modelling of Sea Level Change Contributors, On GRACE satellite gravity data and their application to climate monitoring, Ph.D. thesis, Delft Univ. of Technol., Delft, Netherlands. (Available at <http://www.ncg.knaw.nl/Publicaties/Geodesy/73Wouters.html>)
- Wouters, B., D. Chambers, and E. J. O. Schrama (2008), GRACE observes small-scale mass loss in Greenland, *Geophys. Res. Lett.*, *35*, L20501, doi:10.1029/2008GL034816.
- Wu, X., M. B. Heflin, H. Schotman, B. L. A. Vermeersen, D. Dong, R. S. Gross, E. R. Ivins, A. W. Moore, and S. E. Owen (2010), Simultaneous estimation of global present-day water transport and glacial isostatic adjustment, *Nat. Geosci.*, *3*, 642–646, doi:10.1038/ngeo938.
- Zwally, H. J., M. B. Giovinetto, J. Li, H. G. Cornejo, M. A. Beckley, A. C. Brenner, J. L. Saba, and D. Yi (2005), Mass changes of the Greenland and Antarctic ice sheets and shelves and contributions to sea-level rise: 1992 to 2002, *J. Glaciol.*, *51*(175), 509–527, doi:10.3189/172756505781829007.
-
- E. J. O. Schrama, Faculty of Aerospace Engineering, Delft University of Technology, Kluyverweg 1, NL-2629 HS, Delft, Netherlands. (e.j.o.schrama@tudelft.nl)
- B. Wouters, Koninklijk Nederlands Meteorologisch Instituut, Wilhelminalaan 10, NL-3732 GK De Bilt, Netherlands.